Chapter 2
The *Kepler* Space Photometry Revolution

2.1 Introductory Remarks

In the last few decades, the field of asteroseismology has rapidly expanded and become a widely-known area within astronomy, primarily because of the launch of space-based telescopes. The MOST (Walker et al. 2003) and CoRoT (Auvergne et al. 2009) missions provided a wealth of data on a variety of pulsating stars and paved the way for the more recent *Kepler*Space Telescope (Borucki et al. 2010). These space missions were overwhelmingly successful for asteroseismology and their data remain of great use to this day. Consequently, the decade between the launch of the MOST telescope and the end of the *Kepler*mission has become known as the start of the *Space Photometry Revolution*.[1] An argument can certainly be made that the biggest advances in asteroseismology have been for stars with solar-like oscillations, especially in red giant stars, with $\sim$14 000 being observed by *Kepler*alone (Chaplin and Miglio 2013). Even though asteroseismology of δ Sct stars was possible from the ground, our understanding of these stars has also undoubtedly improved from high-quality space photometry.

This chapter provides an overview of the *Kepler*Space Telescope and its data in Sect. 2.2, with the specifics of Fourier analysis of stellar time series discussed in Sect. 2.3. Section 2.4 contains an overview of how a series of *Kepler*data catalogues were created, which formed the basis of many research projects within the thesis by Bowman (2016).

[1]This was the title of the CoRoT-3/KASC7 conference held in 2014: http://corot3-kasc7.sciencesconf.org. The conference proceedings for a poster by Bowman and Kurtz (2015) were published in the European Physical Journal Web of Conferences (EPJWC) from this conference.

© Springer International Publishing AG 2017

D.M. Bowman, *Amplitude Modulation of Pulsation Modes in Delta Scuti Stars*,
Springer Theses, DOI 10.1007/978-3-319-66649-5_2

2.2 The *Kepler* Space Telescope

The *Kepler*Space Telescope was launched on 7 March 2009 and positioned into a 372.5-d Earth-trailing orbit (Borucki et al. 2010). The field of view covered approximately 115 deg^2 in the constellations of Cygnus and Lyra, within which *Kepler*observed approximately 200 000 stars at an unprecedented photometric precision of a few μmag (Koch et al. 2010). The field of view was chosen with the CCD array positioned so that the brightest stars were in the gaps between CCD modules, with most stars having apparent magnitudes in the *Kepler*passband between $10 \leq \mathrm{Kp} \leq 14$ mag. The primary goal of *Kepler*was to locate Earth-like planets in the habitable zone of their host star using the transit method (Borucki et al. 2010), but these data have also been extremely useful to asteroseismology.

To date, the *Kepler*mission has obtained transit signals for approximately 4500 candidate exoplanets (Borucki et al. 2011), of which about 3500 have been observed using follow-up spectroscopy and confirmed as exoplanets.[2] On the other hand, an argument can be made that *Kepler*was more successful for stellar astronomy with more discoveries and advances made in asteroseismology than exoplanet science. *Kepler*has validated theoretical predictions and made many new and unexpected discoveries. For example, approximately 2900 eclipsing binary systems[3] were observed by *Kepler*(Prša et al. 2011), which allowed the theoretical prediction of tidally induced pulsations made by Kumar et al. (1995) to be tested. Tidal pulsations were first observed in stars in eccentric binary systems using *Kepler*data, creating a group of stars known colloquially as *'Heartbeat stars'*, because of the characteristic shapes of their light curves resembling an echocardiogram (Thompson et al. 2012; Hambleton et al. 2013; Hambleton 2016).

2.2.1 Kepler Instrumentation

The design of the *Kepler*instrument maximises the search for exoplanets orbiting solar-type stars, hence the wavelength response peaks at ∼6000 Å. The wavelength response function for the *Kepler*telescope is plotted in Fig. 2.1 with Johnson filters from Johnson and Morgan (1953) also plotted for comparison (for an extensive review of standard photometric techniques, see Bessell 2005). Using Wien's law, the peak in the *Kepler*response function corresponds to the λ_{max} for a star with an effective temperature of approximately $T_{\mathrm{eff}} \simeq 5000$ K. Therefore, *Kepler*is optimised for studying F, G and K stars. Consequently, *Kepler*observations of oscillations in A stars are suppressed in amplitude from the instrument's passband, but can be corrected

[2] An up-to-date catalogue is available at: http://exoplanetarchive.ipac.caltech.edu.

[3] An up-to-date catalogue is available at: http://keplerebs.villanova.edu.

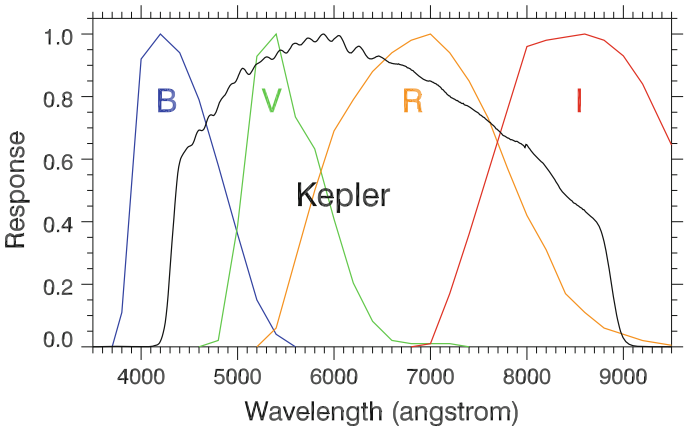


Fig. 2.1 The normalised wavelength response function for the *Kepler*instrument is plotted as the *solid black line* and Johnson B, V, R and I filters taken from Johnson and Morgan (1953) are shown as *coloured solid lines* for comparison

by comparison to other observations (Bowman et al. 2015). This is demonstrated for the δ Sct star KIC 7106205 in Chap. 3.

One of the disadvantages to consider when using broad-band photometry is the restriction of mode visibility. Observations from space telescopes such as *Kepler*are often only sensitive to detecting low-degree ($\ell \leq 2$) pulsation modes, because the amplitudes of high-degree modes are only excited to small amplitudes (Balona and Dziembowski 1999), and because of geometrical cancellation effects (Dziembowski 1977).

2.2.2 *Kepler* Data Characteristics

*Kepler*data are available in long and short cadence (hereafter called LC and SC, respectively), which were created from multiple 6.02-s exposures, each with 0.52-s readout times (Gilliland et al. 2010). The LC data comprised 270 exposures creating a total integration time of 29.45 min, which allowed approximately 170 000 simultaneous observations (Jenkins et al. 2010). The SC data comprised nine exposures creating a total integration time of 58.5 s, which was chosen to increase the temporal resolution, thus increase the number of data points per exoplanet transit of a star. From the limited amount of data storage on board the spacecraft, only 512 stars were observed with SC at any one time (Gilliland et al. 2010). To demonstrate the difference in temporal resolution between LC and SC data, the light curves spanning 1 d of the δ Sct star KIC 71060205 using LC and SC data are shown as blue diamonds and red circles, respectively, in Fig. 2.2.

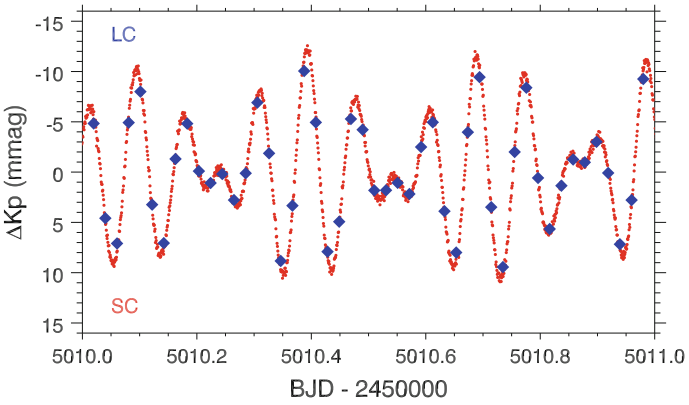


Fig. 2.2 Comparison of LC and SC *Kepler*data spanning 1 d for the δ Sct star KIC 7106205. The SC data have a cadence of 58.5 s and the LC data have a cadence of 29.45 min

To keep its solar panels pointing towards the Sun, the *Kepler*spacecraft had to roll 90 degrees approximately every 93 d — i.e., one quarter of the *Kepler*orbit. The *Kepler*CCD was designed with four-fold symmetry, so a star rotated on the focal plane four times in a *Kepler*year, which is divided into four quarters of LC data. Each quarter was then divided into three months and so SC data are labelled with a quarter and month number. *Kepler*data were stored on board the spacecraft and downloaded to Earth approximately every 31 d. Therefore, *Kepler*data are available as SC months and LC quarters, corresponding to approximately 31 and 93 d, respectively. At the end of the main *Kepler*mission in May 2013, there was a total of 18 LC data quarters each approximately 93 d in length, except for Q0, Q1 and Q17 which were approximately 10, 30 and 30 d, respectively. The length of the complete data set is 1470.5 d, which is just over 4 yr.

Approximately one per cent of all the targets observed by *Kepler*were allocated for asteroseismic research (Gilliland et al. 2010), with a 1-yr proprietary access period given to the *Kepler*Asteroseismic Science Consortium (KASC) via the *Kepler*Asteroseismic Science Operations Center.[4] Today, all *Kepler*light curves in both raw and reduced formats are publicly available from the Mikulski Archive for Space Telescopes (MAST),[5] and are available in two formats. The first type are the raw or unprocessed light curves that are produced using Simple Aperture Photometry (SAP), and the second type are the reduced light curves that are created using a multi-scale Maximum A Prior Pre-Search Data Conditioning (msMAP PDC) pipeline developed by the *Kepler*Science Office — see Smith et al. (2012) and Stumpe et al. (2012) for more details.

The main advantages of using the reduced light curves from the msMAP PDC pipeline over the SAP light curves include: data quarters have been automatically

[4]KASOC website: http://www.kasoc.phys.au.dk.

[5]MAST website: http://archive.stsci.edu/kepler/.

stitched together; the removal of outlying data points; and the removal of systematic sources of instrumental noise. The *Kepler*science pipeline has been developed to optimise the light curves for the detection of exoplanet transit signals and can suppress the amplitudes of long period signals ($P \geq 10$ d). The pipeline does not, however, modify the frequencies of these long-period signals, so the difference for asteroseismology of high-frequency pulsators, such as δ Sct stars, is negligible.

2.2.3 The Kepler Input Catalogue

Approximately 200 000 targets stars were selected to be observed by *Kepler*, with the specific selection criteria discussed by Koch et al. (2010). These targets were characterised with values of $T_{\rm eff}$, log g and [Fe/H] using *griz* and 2MASS *JHK* broad-band photometry prior to the launch of the telescope and were collated into the *Kepler*Input Catalogue (KIC; Brown et al. 2011). Since the end of the nominal *Kepler*mission, Huber et al. (2014) revised the stellar parameters for the ∼200 000 *Kepler*targets and concluded that a colour-dependent offset exists compared to other sources of photometry (e.g., Sloan). This resulted in KIC temperatures for stars hotter than $T_{\rm eff} \gtrsim 6500$ K being, on average, 200 K lower than temperatures obtained from Sloan photometry or the infrared flux method (Pinsonneault et al. 2012). Also, log g values for hot stars were overestimated by up to 0.2 dex. Huber et al. (2014) stress that the $T_{\rm eff}$, log g and [Fe/H] values and their respective uncertainties should not be used for a detailed analysis on a star-by-star basis, as they are only accurate in a statistical sense.

2.2.4 The Failure of Module 3

Approximately 2 yr into the *Kepler*mission, two CCD arrays located on module 3 failed and became inoperative. This resulted in approximately 4/21 of *Kepler*targets not being observed every fourth quarter after this point, because of the rotation of the telescope 90 degrees every ∼93 d. These stars, commonly known as module 3 stars, have a significant gap of ∼90 d in their light curves once per *Kepler*orbit causing more complex window patterns in their amplitude spectra.

2.2.5 K2

In May 2013 the *Kepler*Space Telescope suffered the failure of a second reaction wheel. With only two remaining reaction wheels, the telescope could no longer maintain the necessary level of still-pointing without the significant expenditure of fuel. An ingenious solution was devised by NASA, in which the field of view was

repositioned to point in the direction of the ecliptic, such that torques from the solar radiation pressure were minimised and a smaller amount of fuel was needed to maintain the field of view (Howell et al. 2014). Consequently, the mission parameters have changed and a new mission called K2, *Kepler*'s second light, is underway. K2 data are divided into campaigns, each approximately 80 d in length, with each new campaign observing a variety of targets, including young stars and star-forming regions; supernovae, white dwarfs and the Galactic centre (Howell et al. 2014).

Analysis of K2 data has proved fruitful. Discoveries have included a rare triple-mode RR Lyrae star, EPIC 201585823, with currently only 12 such objects known (Kurtz et al. 2016); an in-depth asteroseismic analysis of O stars for the first time (Buysschaert et al. 2015); and the continued success in finding exoplanets (Vanderburg et al. 2016). The research prospects for asteroseismology using K2 data are good with many more interesting discoveries expected in the next few years. Even though the *Kepler*mission has been redesigned and the telescope is no longer observing the original target stars, the 4 yr of high-quality data will remain a gold mine for scientific discoveries and investigation for many years to come.

2.3 Fourier Analysis of Stellar Time Series

The fundamental data of asteroseismology are the pulsation mode frequencies, which are extracted from time series photometry using Fourier analysis. The Fourier transform (FT) allows one to move from the time domain into the frequency domain by use of

$$F(\nu) = \int_{-\infty}^{+\infty} x(t) e^{2\pi i \nu t} dt \,, \tag{2.1}$$

in which $x(t)$ is a continuous infinite function. The principle of Fourier analysis is that any function can be represented by a summation of sine and cosine functions. In reality, stellar time series are not infinitely long nor are they continuous functions, so the discrete Fourier transform (DFT) described by Deeming (1975) is implemented for finite and discrete data sets. The calculated amplitude spectrum is also convolved with the spectral window of the data set, which is defined by gaps in the data and deviations from a regular cadence (Deeming 1975).

Using the DFT described by Deeming (1975), an amplitude spectrum is calculated using

$$A_i = \left(\frac{2}{N}\right) \sqrt{\left(\sum_{j=0}^{N} x_j(t) \sin(2\pi\nu_i t_j)\right)^2 + \left(\sum_{j=0}^{N} x_j(t) \cos(2\pi\nu_i t_j)\right)^2} \,, \tag{2.2}$$

where A_i is the amplitude at the frequency ν_i calculated from the summation of sine and cosine signals for the discrete time series $x(t)$ with N data points.

2.3.1 The Nyquist Frequency

The Nyquist frequency is the highest frequency that is not undersampled for a given sampling frequency, and is defined as

$$\nu_{\rm Nyq} = \frac{1}{2\Delta t}\,, \tag{2.3}$$

where Δt is the cadence of a discrete data set. For LC *Kepler*data this corresponds to a value of $\nu_{\rm Nyq} = 24.47\ {\rm d}^{-1}$ and for SC data this is $727.35\ {\rm d}^{-1}$. The Nyquist frequency is commonly used as an upper limit in frequency when calculating the amplitude spectrum of a discrete data set because frequencies outside of the range $0 \leq \nu \leq \nu_{\rm Nyq}$ are undersampled and subject to aliasing.

It has been demonstrated that pulsation mode frequencies in δ Sct stars typically lie between $4 \leq \nu \leq 50\ {\rm d}^{-1}$ (Grigahcène et al. 2010; Uytterhoeven et al. 2011; Balona and Dziembowski 2011), thus can exceed the LC *Kepler*Nyquist frequency. Before the advent of the super-Nyquist asteroseismology technique by Murphy et al. (2013), care was needed when extracting frequencies from an amplitude spectrum near or above LC Nyquist frequency because they may be aliases of undersampled frequencies above the Nyquist frequency.

Super-Nyquist Asteroseismology

It was shown by Murphy et al. (2013) using the super-Nyquist asteroseismology (sNa) technique, that real and alias frequencies of pulsation modes can be easily identified in an amplitude spectrum when using *Kepler*data. *Kepler*data were sampled at a regular cadence onboard the spacecraft, but Barycentric time stamp corrections were made to correct for the difference in light arrival time of the photons to the barycentre of the Solar system and to the telescope, respectively, resulting in a non-constant cadence (Murphy et al. 2013). Thus, Nyquist aliases are subject to periodic frequency (phase) modulation with a period equal to the *Kepler*satellite's orbital period of 372.5 d, and consequently have a multiplet structure split by the *Kepler*orbital frequency in an amplitude spectrum (Murphy et al. 2013). The total integrated power is the same for a real peak and its alias multiplet in an amplitude spectrum, but the power of an alias is spread between the central component of the multiplet and its super-Nyquist sidelobes, resulting in a central component with a smaller amplitude when compared to the real peak (Murphy et al. 2013). Therefore, using the sNa technique, real and alias frequencies can often be identified without the need to calculate an amplitude spectrum beyond the LC Nyquist frequency.

To demonstrate the sNa technique described by Murphy et al. (2013), the amplitude spectra for simultaneous LC and SC observations of the HADS star KIC 5950759 have been plotted in the left panel of Fig. 2.3. This HADS star acts as a useful example because of the high S/N of its pulsation modes and because simultaneous LC and SC observations are available. The LC and SC amplitude spectra for KIC 5950759 both show the fundamental radial mode at $\nu_1 = 14.221372\ {\rm d}^{-1}$, and its harmonic $2\nu_{1,{\rm r}} = 28.442744\ {\rm d}^{-1}$ labelled 'r' for real, which lies above the

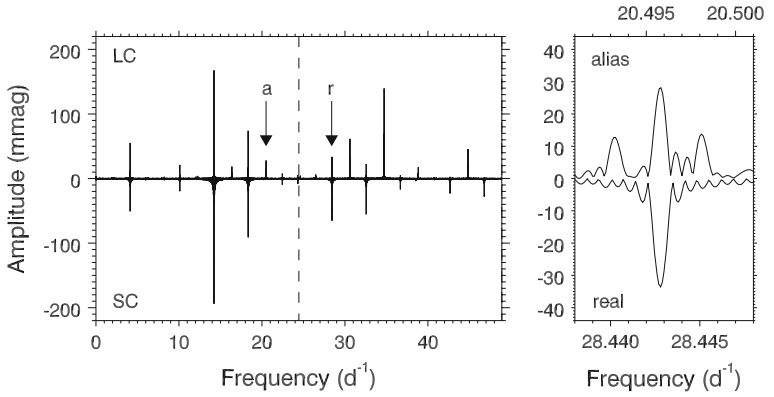


Fig. 2.3 Demonstration of super-Nyquist asteroseismology using the amplitude spectrum of the HADS star KIC 5950759. Real and alias peaks associated with the harmonic of the fundamental radial mode are marked by 'r' and 'a', respectively, in the LC amplitude spectrum in the left panel. The LC Nyquist frequency is indicated by the *vertical dashed line* and the SC amplitude spectrum is shown below for comparison. The *right panel* contains inserts of the LC amplitude spectrum showing the real peak below and the alias peak above. The alias peak is easily identified as its multiplet structure is split by the *Kepler*orbital frequency. Some peaks that exist in the SC amplitude spectrum do not appear in the LC amplitude spectrum as they lie close to the LC sampling frequency and are heavily suppressed in amplitude. Figure from Bowman et al. (2016), their Fig. 2

LC Nyquist frequency indicated by a vertical dashed line in Fig. 2.3. The alias of the harmonic $2\nu_{1,\mathrm{a}} = 20.496203\ \mathrm{d}^{-1}$ can also be seen in the LC amplitude spectrum in Fig. 2.3 and is labelled 'a'. The right panel in Fig. 2.3 shows a zoom-in of the amplitude spectrum using LC data, showing the multiplet structure split by the *Kepler*satellite's orbital frequency of the alias peak in the top panel, compared to the real peak shown below for comparison. Note also, how the amplitude of the alias peak is smaller than the real peak in the LC amplitude spectrum, as predicted by Murphy et al. (2013).

2.3.2 *Frequency Resolution*

It is important to note that SC *Kepler*data does provide a higher temporal resolution, as shown by Fig. 2.2, but does not provide a higher frequency resolution compared to LC observations. The frequency resolution of a data set is given by the Rayleigh resolution criterion of

$$\sigma\left(\nu\right) = \frac{1}{\Delta T}\ , \tag{2.4}$$

where $\sigma\left(\nu\right)$ and ΔT are the frequency resolution and the length of the data set, respectively. A longer time series results in a smaller, and hence improved, frequency resolution, which is represented by the width of the peak in an amplitude spectrum.

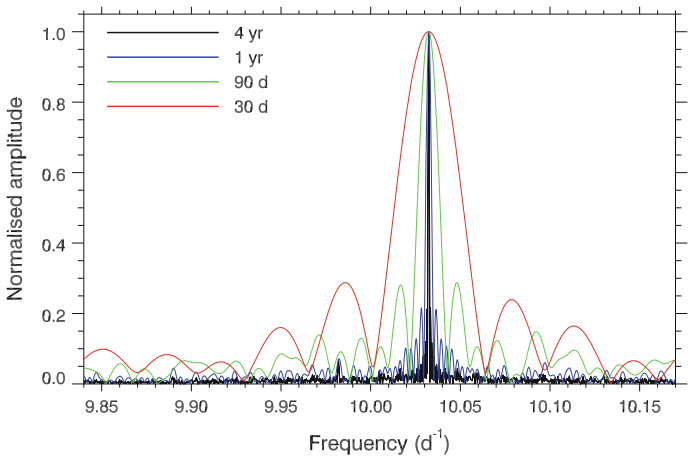


Fig. 2.4 Demonstration of frequency resolution using four different lengths of observations for the pulsation mode frequency at $\nu = 10.0323$ d^{-1} in the δ Sct star KIC 7106205. With a longer time series, a better frequency resolution is obtained, which corresponds to the width of the peak in the amplitude spectrum

This is demonstrated in Fig. 2.4, in which amplitude spectra for time series spanning 30 d, 90 d, 1 yr and 4 yr for a pulsation mode frequency at $\nu = 10.032366$ d^{-1} have been plotted for comparison. As can be seen in Fig. 2.4, the width of the peak is smaller for longer time series following Eq. 2.4. For the 4-yr *Kepler*data set, a frequency resolution of 0.00068 d^{-1} ($\simeq$8 nHz) is obtained.

The relationship in Eq. 2.4 is commonly used in the literature for calculating the frequency resolution of a discrete data set, such as a stellar time series. However, it is not always strictly correct to do so. Loumos and Deeming (1978) analytically derive a frequency resolution of

$$\sigma(\nu) = \frac{3}{2}\,\frac{1}{\Delta T}\,. \tag{2.5}$$

as a more conservative definition of frequency resolution.

Both of the definitions of frequency resolution given in Eqs. 2.4 and 2.5 also only apply for data sets without large gaps. For example, if we take the hypothetical case of two individual time series of a star, each one month in length that are separated by one year, using Eq. 2.4 would yield a frequency resolution of approximately 0.003 d^{-1}, but this is not an appropriate resolution calculation. Mathematically, for data with large gaps, relative to the length of the observations, and also for unequally spaced data, Eq. 2.5 is more appropriate. Loumos and Deeming (1978), show for the hypothetical scenario described here, the frequency resolution of two months of data separated by one year, is no better than the resolution obtained from a single month of observations.

2.3.3 Amplitude Visibility Function

It was discussed in Sect. 2.3.2 how the length of a data set determines the frequency resolution in an amplitude spectrum and is independent of the cadence, such that the width of a peak in an amplitude spectrum is the same for both LC and SC observations of the same length. However, the longer integration times of the LC data reduce the amplitudes of peaks in an amplitude spectrum compared to SC data, which is also a strong function of frequency. The exact functional form of the amplitude suppression caused by integration time is given by the amplitude visibility function in Eq. 2.6. The derivation of this equation is given below and was described by Murphy (2014).

In Fig. 2.5 a periodic flux variation of frequency $\nu = 10.0\,\mathrm{d}^{-1}$ is shown by the solid blue line and the interval between consecutive data points in LC *Kepler*data is shown by the width of the green-hatched rectangle, δ. The height of the rectangle is the area divided by its width, thus for the same frequency signal a shorter sampling would produce a taller and narrower rectangle in Fig. 2.5. Assuming that the $\nu = 10.0\,\mathrm{d}^{-1}$ signal is periodic and has the form $\cos(\omega t)$, then the height of the rectangle, H, is given by:

$$
\begin{aligned}
&= \frac{1}{\delta} \int_{t_0 - \frac{\delta}{2}}^{t_0 + \frac{\delta}{2}} \cos(\omega t) dt \\
&= \frac{1}{\delta} \frac{1}{\omega} \left\{ \sin\left[\omega \left(t_0 + \frac{\delta}{2} \right) \right] - \sin\left[\omega \left(t_0 - \frac{\delta}{2} \right) \right] \right\} .
\end{aligned}
$$

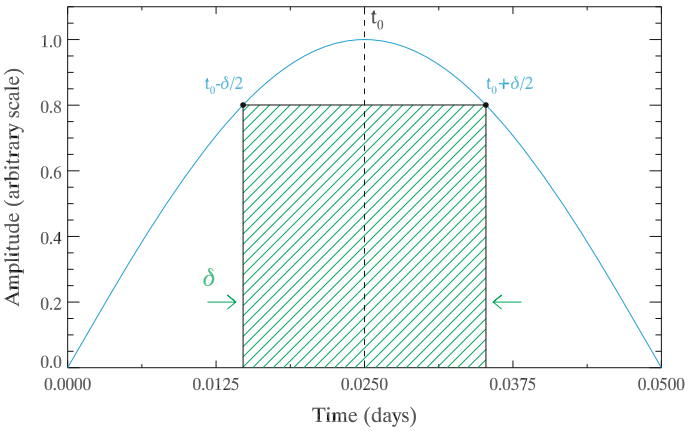


Fig. 2.5 Demonstration of how longer integration times lead to an underestimate in amplitude of a periodic signal. A frequency of $\nu = 10.0\,\mathrm{d}^{-1}$ is shown as the *solid blue line* and the interval between consecutive data points is given by δ, which is symmetric from a reference time, t_0, and has been chosen to emulate the LC *Kepler*sampling frequency. With a shorter integration time, δ, less amplitude suppression occurs as the height of the rectangle increases and approaches the true amplitude of unity in this example. Figure from Murphy (2014), his Fig. 1.4. Reproduced with kind permission from author

This can be re-written using the trigonometric identity $\sin(X+Y) = \sin X \cos Y + \cos X \sin Y$, as:

$$
\begin{aligned}
&= \frac{1}{\delta}\frac{1}{\omega}\left[\sin(\omega t_0)\cos\left(\frac{\omega\delta}{2}\right) + \cos(\omega t_0)\sin\left(\frac{\omega\delta}{2}\right)\right. \\
&\qquad \left. - \sin(\omega t_0)\cos\left(\frac{\omega\delta}{2}\right) + \cos(\omega t_0)\sin\left(\frac{\omega\delta}{2}\right)\right] \\
&= \frac{1}{\omega\delta}\left[2\cos(\omega t_0)\sin\left(\frac{\omega\delta}{2}\right)\right] \\
&= \cos(\omega t_0)\,\mathrm{sinc}\left(\frac{\omega\delta}{2}\right) .
\end{aligned}
$$

Using the relationship between angular frequency and period, $\omega = \frac{2\pi}{P}$, with P being the period of the signal, and that the time interval between consecutive data points is related to the number of data points per cycle, $\delta = \frac{P}{n}$, the above can be rewritten as

$$A = A_0\,\mathrm{sinc}\left(\frac{\pi}{n}\right) = A_0\,\mathrm{sinc}\left(\frac{\pi\nu}{\nu_{\mathrm{samp}}}\right), \tag{2.6}$$

where A is the observed amplitude, A_0 is the true amplitude, n is the number of data points per pulsation cycle, ν is the pulsation mode frequency and ν_{samp} is the instrumental sampling frequency. From the relationship in Eq. 2.6, it can be seen that higher frequency signals are, on average, more heavily suppressed in amplitude, but only exactly integer multiples of the LC sampling frequency, $\nu_{\mathrm{samp}} = 48.9\ \mathrm{d}^{-1}$, are completely suppressed, which is shown graphically in Fig. 2.6. Therefore, from the

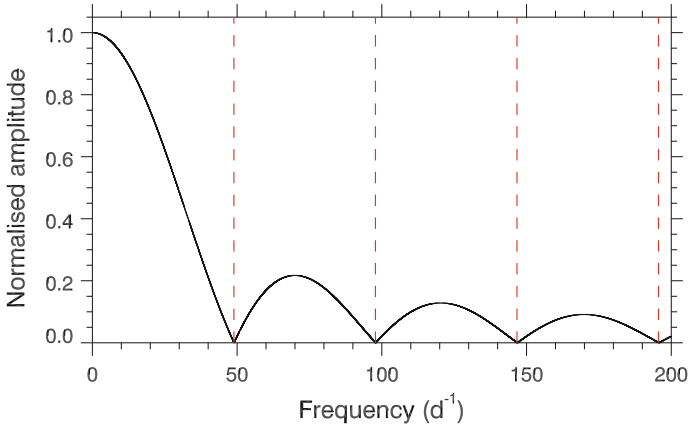


Fig. 2.6 The amplitude visibility function as a function of frequency for LC *Kepler*data. Higher frequencies are suppressed heavily in amplitude because there are fewer data points per pulsation cycle, n, but only frequencies equal to integer multiples of the sampling frequency are completely suppressed. The *vertical red dashed lines* indicate integer multiples of the LC sampling frequency $\nu_{\mathrm{samp}} = 48.9\ \mathrm{d}^{-1}$

shorter integration times, SC data will produce a higher amplitude peak for a given frequency compared to LC data.

2.4 *Kepler* Data Catalogues

One of the first tasks undertaken as part of the thesis by Bowman (2016) was to identify all the pulsating A and F stars, specifically the δ Sct stars, observed by the *Kepler*Space Telescope. Although the *Kepler*instrument is optimised for observing solar-type stars, several thousand A and F stars were included in the 200 000 target stars. In this section, the downloading and processing of light curves for all A and F stars, and the methodology of producing the *Kepler*data catalogues is discussed.

2.4.1 Creating Data Catalogues

To create a statistical ensemble of δ Sct stars, the light curves produced by the msMAP PDC pipeline (Stumpe et al. 2012; Smith et al. 2012) for all *Kepler*targets with effective temperatures between $6400 \leq T_{\rm eff} \leq 10\,000$ K in the KIC were downloaded from MAST. The extracted time series were stored locally in the format of reduced Barycentric Julian Date (BJD $-$ 2 400 000) and stellar magnitudes, which were normalised for each quarter of LC and month of SC data to be zero in the mean. This resulted in approximately 10 400 stars within this $T_{\rm eff}$ range. Examples of the file format for the first LC quarter and first SC month of the fictitious star KIC 1234567 are

```
kic001234567_Q00_LC.txt
kic001234567_Q00_M1_SC.txt
```

The time series were separated into temperature bins for parallelised computing with the number of stars in each temperature bin shown in Table 2.1. The range of the temperature bins is somewhat arbitrary, but was chosen to create bins with similar number of stars and type of pulsator. For example, the overlapping region of the δ Sct and γ Dor instability regions is approximately between $6800 \leq T_{\rm eff} \leq 8000$ K, and so it was important to separate these stars into three groups. Similarly, the hot δ Sct and cool γ Dor stars have separate groups. Thus, considering that typical uncertainties for stars with $T_{\rm eff} \simeq 6500$ K and $T_{\rm eff} \simeq 9000$ K are approximately ± 150 and ± 400 K, respectively, all the stars within a bin can be considered as having the same effective temperature.

An automated pipeline was created to calculate the amplitude spectrum for each LC quarter for each star. The method for calculating the Fourier transform of a discrete data series is described in detail by Deeming (1975), and was optimised for faster computation time by Kurtz (1985). These tools were checked and found to

Table 2.1 The number of stars downloaded from MAST for each temperature bin as listed in the KIC (Brown et al. 2011) is given, indicating fewer hot stars than cool stars

KIC temperature (K)	Number	Spectral type	Comment
$9000 \leq T_{\rm eff} < 10\,000$	329	A1 – A3	
$8000 \leq T_{\rm eff} < 9000$	907	A3 – A6	δ Sct blue edge
$7500 \leq T_{\rm eff} < 8000$	912	A6 – A7	γ Dor blue edge
$7000 \leq T_{\rm eff} < 7500$	1587	A8 – F0	
$6800 \leq T_{\rm eff} < 7000$	1129	F0 – F2	δ Sct red edge
$6600 \leq T_{\rm eff} < 6800$	1752	F3 – F4	
$6500 \leq T_{\rm eff} < 6600$	1754	F4 – F5	γ Dor red edge
$6400 \leq T_{\rm eff} < 6500$	2025	F5 – F6	
Total	10 395		

be consistent with the frequency software package `PERIOD04` (Lenz and Breger 2005).

2.4.2 *Kepler* Data Catalogue Extract

The light curves and amplitude spectra have been collated into a series of PDF catalogues, one for each of the effective temperature bins given in Table 2.1. At the top of each page in a data catalogue, a star's unique *Kepler*ID number starting with the characters KIC (*Kepler*Input Catalogue) and its stellar parameters listed in the KIC (Brown et al. 2011) are given. Next to the KIC ID number, the LC data quarter number is also given. The light curve is shown in the top panel, which have all been set to be zero in the mean and have ordinate units of mmag. The middle panel shows the LC amplitude spectrum calculated out to the Nyquist frequency, and the bottom panel shows a zoom-in of the low-frequency regime in the amplitude spectrum at the same ordinate scale but a smaller abscissa scale. The third panel shows the expected frequency range for g modes, specifically $0 \leq \nu \leq 6\,{\rm d}^{-1}$, and was chosen to show any longer periodicity present in the amplitude spectrum as a separate plot since many δ Sct stars have peaks in the low-frequency regime (see e.g., Grigahcène et al. 2010; Uytterhoeven et al. 2011; Balona 2011). The ordinate scale in every page (i.e., for all LC data quarters) of each star is kept fixed, thus one can see changes in amplitude of the pulsation modes more easily.

The Figs. 2.7 and 2.8 are extracts from the $6800 \leq T_{\rm eff} \leq 7000$ K *Kepler*data catalogue showing Q0 and Q17, respectively, for the δ Sct star KIC 7106205. Scrolling through the *Kepler*data quarters on separate pages of the data catalogues allowed KIC 7106205 to be quickly identified as a δ Sct star with significant amplitude modulation, and motivated the analysis of this star by Bowman and Kurtz (2014), which

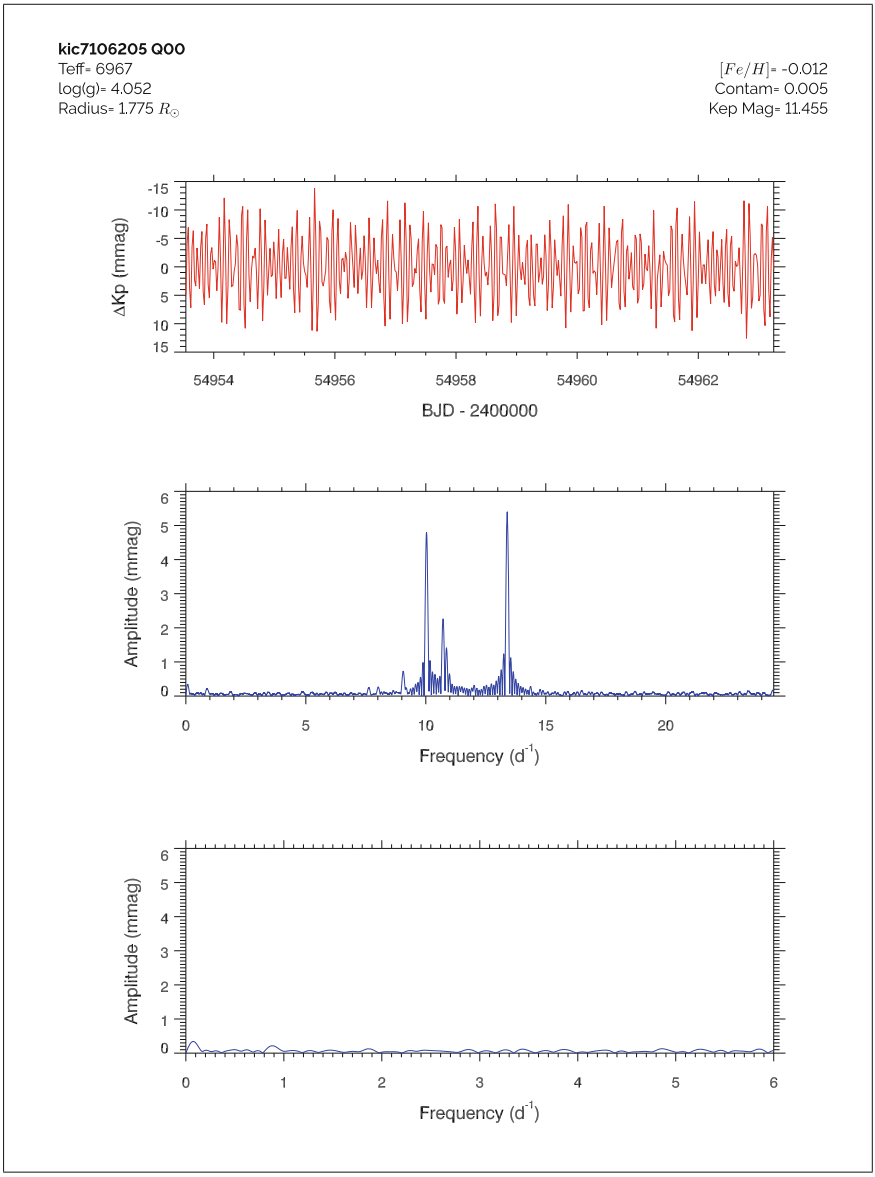


Fig. 2.7 An example page from the *Kepler*data catalogue for Q0 of the δ Sct star KIC 7106205

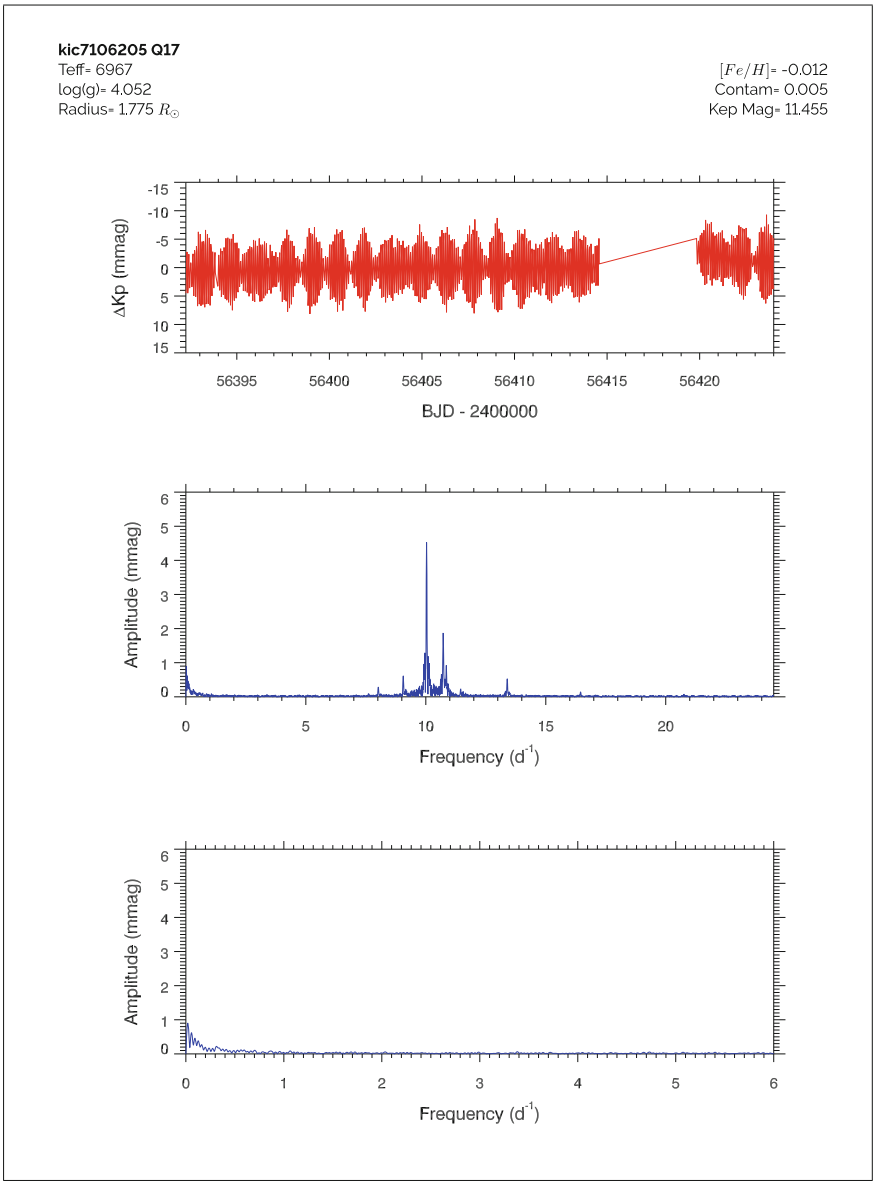


Fig. 2.8 An example page from the *Kepler*data catalogue for Q17 of the δ Sct star KIC 7106205

is discussed in Chap. 3. Specifically, it was the significant decrease in the amplitude of the peak at $\nu \simeq 13.5\ \mathrm{d}^{-1}$ from Q0 to Q17 that is most noticeable.

2.5 Discussion

The advent of space-based telescopes in the last decade such as MOST (Walker et al. 2003), CoRoT (Auvergne et al. 2009) and *Kepler*(Borucki et al. 2010), has become known as the Space Photometry Revolution. The *Kepler*Space Telescope provided high photometric precision, a high duty cycle and data spanning years for 200 000 stars (Koch et al. 2010). Although the mission was designed to find Earth-like exoplanets orbiting solar-type stars using the transit method, these data have also been extremely useful for studying pulsating stars using asteroseismology.

In this chapter, a review of *Kepler*instrumentation has been provided, including a discussion of the main differences in SC and LC data and the implications for asteroseismology. Specifically, the 29.5-min cadence of LC *Kepler*data may have the same frequency resolution for the same length of SC data according to the Rayleigh resolution criterion, but it was shown that the amplitude suppression from the longer integration time is an important factor to consider when interpreting an amplitude spectrum. From the complete 4-yr *Kepler*data set, a frequency resolution of $0.00068\ \mathrm{d}^{-1}$ ($\simeq$8 nHz) and an amplitude precision of order a few μmag is obtained, which are important for studying the changes in the pulsation modes over time – i.e., frequency and amplitude modulation – in pulsating stars such as δ Sct stars.

In this chapter, it was discussed how a total of approximately 10 400 stars with effective temperatures between $6400 \leq T_{\mathrm{eff}} \leq 10\,000$ K observed by *Kepler*were downloaded and processed into *Kepler*data catalogues. These catalogues represent a valuable tool for quickly and efficiently identifying different types of pulsating stars observed by *Kepler*, as one is able to simply search for pulsation modes in the frequency range of interest. The ordinate axis of the amplitude spectra was chosen to be fixed for each LC quarter of each star, such that significant amplitude modulation in δ Sct stars could easily be identified.

The usefulness of these data catalogues was demonstrated for the δ Sct star KIC 7106205 in Sect. 2.4.2, which led to the study of amplitude modulation in this star by Bowman and Kurtz (2014) and Bowman et al. (2015) presented in Chap. 3. The *Kepler*data catalogues discussed in this chapter will remain of great use for years to come, as the 4-yr length of *Kepler*data will not be surpassed in the foreseeable future.

References

Auvergne, M., Bodin, P., Boisnard, L., et al. 2009, A&A, 506, 411
Balona, L. A. 2011, MNRAS, 415, 1691
Balona, L. A. & Dziembowski, W. A. 1999, MNRAS, 309, 221
Balona, L. A. & Dziembowski, W. A. 2011, MNRAS, 417, 591
Bessell, M. S. 2005, ARA&A, 43, 293
Borucki, W. J., Koch, D., Basri, G., et al. 2010, Science, 327, 977
Borucki, W. J., Koch, D. G., Basri, G., et al. 2011, ApJ, 728, 117
Bowman, D. M. 2016, PhD thesis, Jeremiah Horrocks Institute, University of Central Lancashire, UK
Bowman, D. M. & Kurtz, D. W. 2014, MNRAS, 444, 1909
Bowman, D. M. & Kurtz, D. W. 2015, in European Physical Journal Web of Conferences, Vol. 101, European Physical Journal Web of Conferences, 6013
Bowman, D. M., Holdsworth, D. L., & Kurtz, D. W. 2015, MNRAS, 449, 1004
Bowman, D. M., Kurtz, D. W., Breger, M., Murphy, S. J., & Holdsworth, D. L. 2016, MNRAS, 460, 1970
Brown, T. M., Latham, D. W., Everett, M. E., & Esquerdo, G. A. 2011, AJ, 142, 112
Buysschaert, B., Aerts, C., Bloemen, S., et al. 2015, MNRAS, 453, 89
Chaplin, W. J. & Miglio, A. 2013, ARA&A, 51, 353
Deeming, T. J. 1975, Ap&SS, 36, 137
Dziembowski, W. 1977, Acta Astronomica, 27, 203
Gilliland, R. L., Brown, T. M., Christensen-Dalsgaard, J., et al. 2010, PASP, 122, 131
Grigahcène, A., Antoci, V., Balona, L., et al. 2010, ApJL, 713, L192
Hambleton, K. M. 2016, PhD thesis, Jeremiah Horrocks Institute, University of Central Lancashire, UK
Hambleton, K. M., Kurtz, D. W., Prša, A., et al. 2013, MNRAS, 434, 925
Howell, S. B., Sobeck, C., Haas, M., et al. 2014, PASP, 126, 398
Huber, D., Silva Aguirre, V., Matthews, J. M., et al. 2014, ApJS, 211, 2
Jenkins, J. M., Caldwell, D. A., Chandrasekaran, H., et al. 2010, ApJL, 713, L87
Johnson, H. L. & Morgan, W. W. 1953, ApJ, 117, 313
Koch, D. G., Borucki, W. J., Basri, G., et al. 2010, ApJL, 713, L79
Kumar, P., Ao, C. O., & Quataert, E. J. 1995, ApJ, 449, 294
Kurtz, D. W. 1985, MNRAS, 213, 773
Kurtz, D. W., Bowman, D. M., Ebo, S. J., et al. 2016, MNRAS, 455, 1237
Lenz, P. & Breger, M. 2005, Communications in Asteroseismology, 146, 53
Loumos, G. L. & Deeming, T. J. 1978, Ap&SS, 56, 285
Murphy, S. J. 2014, PhD thesis, Jeremiah Horrocks Institute, University of Central Lancashire, UK
Murphy, S. J., Shibahashi, H., & Kurtz, D. W. 2013, MNRAS, 430, 2986
Pinsonneault, M. H., An, D., Molenda-Żakowicz, J., et al. 2012, ApJS, 199, 30
Prša, A., Batalha, N., Slawson, R. W., et al. 2011, AJ, 141, 83
Smith, J. C., Stumpe, M. C., Van Cleve, J. E., et al. 2012, PASP, 124, 1000
Stumpe, M. C., Smith, J. C., Van Cleve, J. E., et al. 2012, PASP, 124, 985
Thompson, S. E., Everett, M., Mullally, F., et al. 2012, ApJ, 753, 86
Uytterhoeven, K., Moya, A., Grigahcène, A., et al. 2011, A&A, 534, A125
Vanderburg, A., Latham, D. W., Buchhave, L. A., et al. 2016, ApJS, 222, 14
Walker, G., Matthews, J., Kuschnig, R., et al. 2003, PASP, 115, 1023

http://www.springer.com/978-3-319-66648-8

Amplitude Modulation of Pulsation Modes in Delta Scuti Stars

Bowman , D.

2017, XVI, 204 p. 83 illus., 62 illus. in color., Hardcover
ISBN: 978-3-319-66648-8